DISTRIBUTION OF POTENTIAL OLIVINE SITES ON THE SURFACE OF VESTA BY DAWN FC.

A. Nathues[1], M. Hoffmann[1], M. Schäfer[1], G. Thangjam[1], V. Reddy[2,1], E. A. Cloutis[3], K. Mengel[4], U. Christensen[1], H. Sierks[1], L. Le Corre[3], J. B. Vincent[1], C. T. Russell[5], C. Raymond[6], [1]Max Planck Institute for Solar System Research, Katlenburg-Lindau, Germany, [2]Planetary Science Institute, Tucson, Arizona, USA, [3]University of Winnipeg, Canada, [4]Clausthal University of Technology, Clausthal-Zellerfeld, Germany, [5]University of California, Los Angeles, USA, [6]Jet Propulsion Laboratory, Pasadena, USA; (nathues@mps.mpg.de).

Introduction: The Dawn Framing Camera (FC) [1] has imaged the entire visible surface of Vesta from three different orbits at spatial resolutions of ~250 m/pixel, ~60 m/pixel, and ~20 m/pixel. The FC is equipped with one clear and seven color filters, covering the wavelength range between 0.44 and 1.0 µm [1].

Vesta is geologically the most diverse differentiated basaltic asteroid that survived the collisional history of the Solar System [2]. Most of the howardite-eucrite-diogenite (HED) meteorites found on Earth are likely samples from Vesta and the Vestoids [3, 4]. Several models, based on the petrogenesis of HEDs [5, 6], favor the evolution of Vesta through a magma ocean. However, the variance of incompatible trace elements among diogenites also supports the serial magmatism model [7, 8]. In order to prove and constrain the existing evolution models we started an extensive lithologic mapping effort of the Vestan surface [9]. During the first months at Vesta the Dawn spacecraft was able to confirm the HED-dominated lithologies [10, 11] while potential mantle material was only recently detected in the craters Bellicia and Arruntia [12,13].

The differentiation of Vesta has presumably led to the formation of a mantle rich in olivine. The crust, however, is assumed to be olivine-free, but at the transition from mantle to crust, a transition from olivine rich dunites to olivine poor diogenites can be observed if samples are exposed on the surface by deep impacts. Here we present the latest results of our global Vesta mapping campaign using FC color data with the focus on the detection of potential olivine sites.

Data Processing: FC images exist in three standard levels from which we use level 1c that is corrected for the "in-field" stray light component [14]. Level 1c I/F data is used for processing in our ISIS pipeline [15], which performs the photometric correction of the FC color data to standard viewing geometry using Hapke functions. The resulting reflectance data are map-projected in several steps, and co-registered to align the color frames, creating color cubes. For the present analysis, FC color data from HAMO and HAMO_2 orbits were used. The color mosaics generated by the ISIS pipeline were analyzed using ENVI and ArcGIS software. For the photometric correction of our FC data and the visualization of the results, we used the Vesta shape model (gaskell_vesta_20130522_dem.cub) derived from FC clear filter images [16].

First Results: Spectral parameters which are suited to identifying potential olivine concentrations >40% have been described by [13]. The parameter set consists of the following spectral information:

Band Tilt (BT) = $(R_{0.92\mu m} / R_{0.96\mu m})$

Mid Ratio (MR) = $(R_{0.75\mu m} / R_{0.83\mu m}) / (R_{0.83\mu m} / R_{0.92\mu m})$

Mid Curvature (MC) = $(R_{0.75\mu m} + R_{0.92\mu m}) / R_{0.83\mu m}$;

where $R(\lambda)$ is the reflectance in the corresponding filter.

In this parameter set the shape of the olivine's 1-µm absorption band in contrast to the pyroxene absorption with its slightly shorter central wavelength is used. The primary criterion for olivine is the ratio BT, which does not reach values considerably higher than 1.0 for HED-dominated lithologies.

In order to be able to create an olivine distribution map of Vesta, we initially identified those areas showing BT values >1.03. Sites with at least 4 contiguous FC pixels were assumed to be significant. Cubes with obvious degraded quality because of rough topography have been discarded.

Our preliminary olivine distribution map is presented in Figure 1. As one can see, the potential olivine sites are unevenly distributed across the Vestan surface. The most prominent concentration is in the northern hemisphere between 30° and 150° longitude. Among these are the craters Bellicia, Pomponia (Figs. 2 and 3), and Arruntia. Interestingly, we have only a few identifications of potential olivine-bearing sites for the deep southern basins, e.g., at craters Tarpeia, Tuccia, Sossia, and some unnamed sites. Furthermore, most of these sites are not located at the lowest topographic areas, but instead on the inner crater wall close to the pre-impact surface level. We also found that many of the potential olivine bearing sites are embedded in diogenitic lithologies, which would be in accordance with a crust/mantle boundary origin. Olivine has been detected in areas much smaller than their host craters, which are of the order of tens of kilometers in diameter. These sites are also characterized by downslope motion. Consequently much of the olivine has been mixed with its environment.

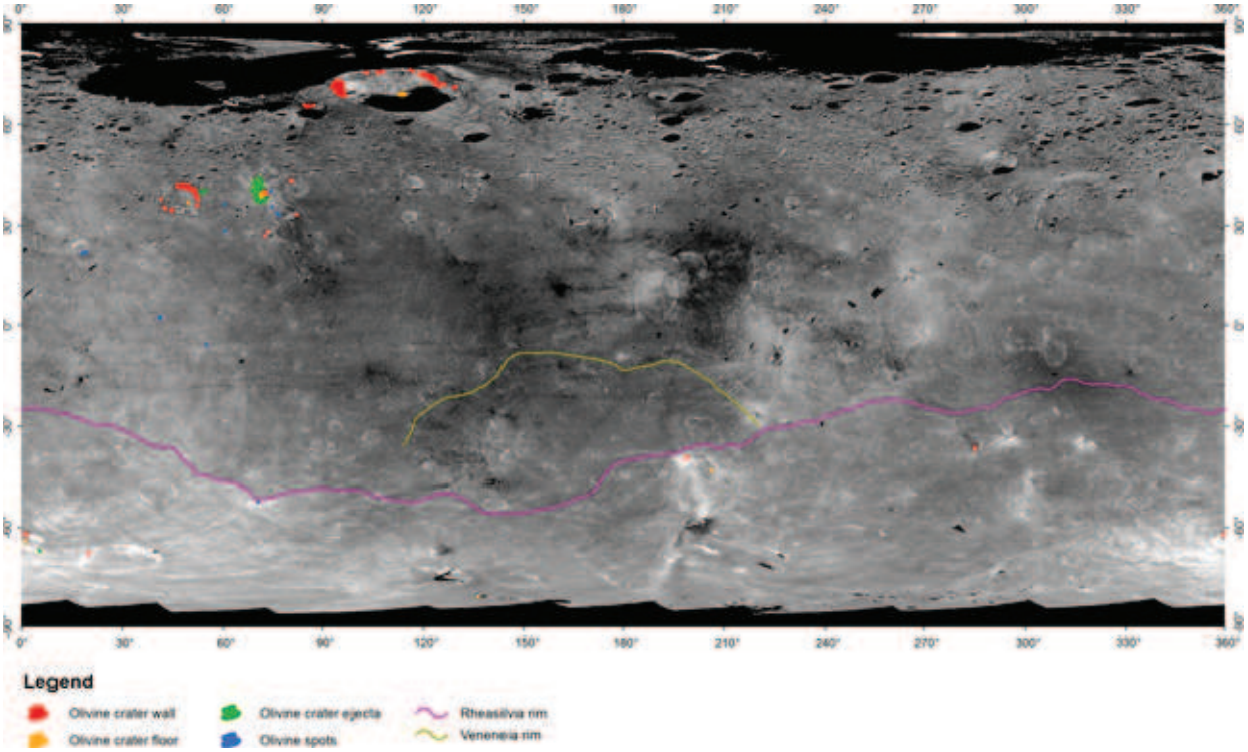

Fig. 1: Global map of potential olivine sites from FC.

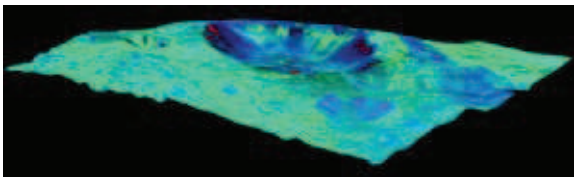

Fig. 2: 3D view of potential olivine sites (red) in crater Pomponia.

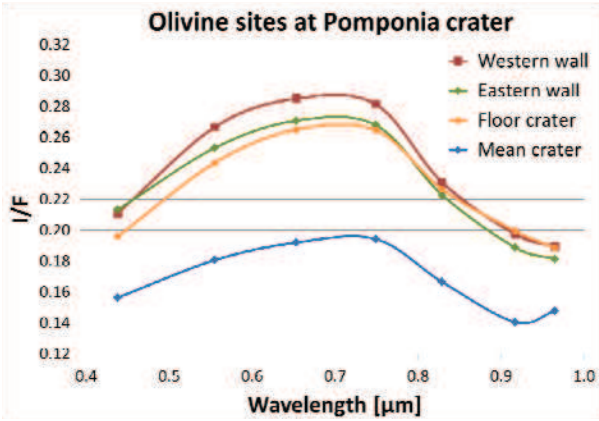

Fig. 3: Potential olivine spectra (red, green, yellow) at crater Pomponia.

Conclusion: Although the Dawn FC data are restricted to wavelengths shorter than 1 µm the identification of potential olivine-bearing sites is feasible [13]. We have likely identified olivine on Vesta at many sites, but its distribution and exact location is not well understood until now. We intend to finalize our olivine mapping of the Vestan surface by the time of the LPSC 2014 and report about the most recent findings.

References:

[1] Sierks H. et al. (2011) *Space Sci. Rev., 163,* 263-327. [2] Russell C. T. et al. (2012) *Science, 336,* 684-686. [3] McCord T. B. et al. (1970) *Science, 178,* 745-747. [4] Schenck P. et al. (2012) *Science, 336,* 694-697. [5] Righter K. and Drake M. J. (1997) *Meteoritics & Planet. Sci., 32,* 929-944. [6] Ruzicka A. et al. (1997) *Meteoritics & Planet. Sci., 32,* 825-840. [7] Mittlefehldt D. W. (1994) *Geochim. Cosmochim. Acta, 58,* 1537-1552. [8] Fowler G. W. et al. (1995) *Geochim. Cosmochim. Acta, 59,* 3071-3084. [9] Thangjam G. et al. (2013) *Meteoritics & Planet. Sci., 48,* 2199-2210. [10] Reddy V. et al. (2012) *Science, 336,* 700-704. [11] De Sanctis M. C. et al. (2012) *Science, 336,* 697-700. [12] Ammanito E. et al. (2013) *Nature, 504,* 122-125. [13] Thangjam G. et al. (2014) *LPS XLV,* Abstract. [14] Kovacs G. et al. (2013) *Proc. SPIE* 8889. [15] Anderson J. A. et al. (2004) *LPS XXXV,* (Abstract#2039). [16] Gaskell R. W. (2012) *AAS, DPS meeting XLIV,* (Abstract #209.03).